

# A New Dust Budget In The Large Magellanic Cloud

Chunhua Zhu<sup>1</sup>, Guoliang Lü<sup>1\*</sup>, Zhaojun Wang<sup>1</sup>

<sup>1</sup>*School of Physics, Xinjiang University, Urumqi, 830046, China*

2 March 2024

## ABSTRACT

The origin of dust in a galaxy is poorly understood. Recently, the surveys of the Large Magellanic Cloud (LMC) provide astrophysical laboratories for the dust studies. By a method of population synthesis, we investigate the contributions of dust produced by asymptotic giant branch (AGB) stars, common envelope (CE) ejecta and type II supernovae (SNe II) to the total dust budget in the LMC. Based on our models, the dust production rates (DPRs) of AGB stars in the LMC are between about  $2.5 \times 10^{-5}$  and  $4.0 \times 10^{-6} M_{\odot} \text{yr}^{-1}$ . The uncertainty mainly results from different models for the dust yields of AGB stars. The DPRs of CE ejecta are about  $6.3 \times 10^{-6}$  (The initial binary fraction is 50%). These results are within the large scatter of several observational estimates. AGB stars mainly produce carbon grains, which is consistent with the observations. Most of dust grains manufactured by CE ejecta are silicate and iron grains. The contributions of SNe II are very uncertain. Compared with SNe II without reverse shock, the DPRs of AGB stars and CE ejecta are negligible. However, if only 2 % of dust grains produced by SNe II can survive after reverse shock, the contributions of SNe II are very small. The total dust masses produced by AGB stars in the LMC are between  $2.8 \times 10^4$  and  $3.2 \times 10^5 M_{\odot}$ , and those produced by CE ejecta are about  $6.3 \times 10^4$ . They are much lower than the values estimated by observations. Therefore, there should be other dust sources in the LMC.

**Key words:** binaries: close stars: evolution circumstellar matter dust

## 1 INTRODUCTION

The interstellar medium (ISM) of a galaxy, one of the drivers of itself evolution, determines many characteristics of the stars forming in it. Dust is one of the important ingredients of the ISM, and plays a central role in the astrophysics of the ISM. However, the dust origin in the ISM is less understood. According to a popular point of view, the stellar winds of asymptotic giant branch (AGB) stars and type II supernovae (SNe II) ejecta have long been considered the main sites of dust formation (e.g., Gail et al. 2009; Dunne et al. 2003; Gall et al. 2011). In addition, red supergiants, luminous blue variables, Wolf-Rayet stars and type Ia supernovae can also produce dust (e.g., Massey et al. 2005; McDonald et al. 2009, 2011; Borkowski et al. 2006; Nozawa et al. 2011). However, compared with AGB stars and SNe II, their contributions to the dust production are negligible (e.g., Zhukovska et al. 2008; Gall et al. 2011).

Recently, as an ideal laboratory for dust formation and evolution, the Large Magellanic Cloud (LMC) was observed by a number of surveys which detected the IR dust emissions from stellar sources (e.g., Cioni et al. 2000; Egan et al.

2001; Meixner et al. 2006; Blum et al. 2006; Ita et al. 2008; Shimonishi et al. 2013). Based on the observations from the *Spitzer Space Telescope*, Matsuura et al. (2009) carried out the measurement of the dust production rate (DPR) by stars for the entire LMC. They estimated that the DPR of carbon-rich (C-rich) AGB stars is  $\sim 4.3 \times 10^{-5} M_{\odot} \text{yr}^{-1}$ , much higher than that of oxygen-rich (O-rich) AGB stars (up to  $\sim 1.7 \times 10^{-5} M_{\odot} \text{yr}^{-1}$ ). Based on the best fit Grid of Red Supergiant and Asymptotic Giant Branch Models, Riebel et al. (2012) estimated that DPR by C-rich AGB stars is  $\sim 1.3\text{--}1.4 \times 10^{-5} M_{\odot} \text{yr}^{-1}$ , which is two and a half times as much dust into the ISM as do O-rich AGB stars. Very recently, based on the evolutionary models of stars through the AGB phase, Dell’Agli et al. (2014, 2015) interpreted the *Spitzer* observations of extreme stars and AGB stars in the LMC. Theoretically, according to the model for dust-mass returned from AGB stars, Zhukovska & Henning (2013) calculated the DPR of AGB stars in the LMC. They found that DPR by C-rich AGB stars is  $\sim 5.7 \times 10^{-5} M_{\odot} \text{yr}^{-1}$ , and DPR by O-rich AGB stars is only  $\sim 1.3 \times 10^{-6} M_{\odot} \text{yr}^{-1}$ . Similarly, using the grids of dust yields for different stellar masses and metallicities calculated by Ventura et al. (2012), Ventura et al. (2012), Di Criscienzo et al. (2013), and Ventura et al. (2014), Schneider et al. (2014) found that

\* E-mail: guolianglv@xao.ac.cn (LGL)

DPR by C-rich AGB stars is  $\sim 4.0 \times 10^{-5} M_{\odot} \text{ yr}^{-1}$  ( $\sim 3.0 \times 10^{-6} M_{\odot} \text{ yr}^{-1}$ ) and DPR by O-rich AGB stars is  $\sim 6.0 \times 10^{-6} M_{\odot} \text{ yr}^{-1}$  ( $\sim 6.0 \times 10^{-6} M_{\odot} \text{ yr}^{-1}$ ), respectively.

The chemical composition of the dust mixture from AGB stars is determined by the carbon-to-oxygen element abundance ratio ( $C/O$ ) in the stellar wind. In O-rich environment ( $C/O < 1$ ), dust produced is mainly silicate, while amorphous carbon dust is dominantly formed in C-rich environment ( $C/O > 1$ ). Based on the above observational and theoretical results, dust in the LMC should be mainly composed of amorphous carbon grains, and the silicate grains account for a small part. However, Weingartner & Draine (2001) estimated the total volume per H atom in the carbonaceous and silicate grain populations in the Milk Way, LMC and SMC. The volumes per H atom of the carbonaceous and silicate grain in the LMC are  $\sim 0.4 \times 10^{-27} \text{ cm}^3 \text{ H}^{-1}$  and  $\sim 1.3 \times 10^{-27} \text{ cm}^3 \text{ H}^{-1}$ , respectively. Considering the ideal graphite density of  $2.24 \text{ g cm}^{-3}$  and the silicate density of  $3.5 \text{ g cm}^{-3}$ , we estimate that the mass ratio of carbon to silicate grains in the LMC is about 1:4.

Therefore, most of silicate grains may not be produced by AGB stars. Are they produced by SNe II ejecta? Unfortunately, it is presently not definitely known how much dust is produced by SNe II ejecta. Zhukovska et al. (2008) simulated the dust returned by different sources in the solar neighbourhood. They found that the dust grains produced by SN ejecta mainly are carbonaceous grains, while the number of silicate grains is negligible. It is possible that most of silicate grains do not originate from SN ejecta. Draine & Salpeter (1979) put forward that dust can grow in the ISM (also see Draine 2009). Unfortunately, the destruction and growth processes of dust in the ISM are poorly understood, and it is very difficult to observe them (e.g., Dwek et al. 2007).

Recently, Lü et al. (2013) suggested that the common envelope (CE) ejecta in close binary systems can provide a favourable environment for dust formation and growth. Very recently, Nicholls et al. (2013) showed that V1309 Sco had become dominated by mid-IR emission since eruption, which indicated the presence of a significant amount of dust in the circumstellar environment. Zhu et al. (2013) considered that these dust grains around V1309 Sco were efficiently produced in its progenitor-binary-merger ejecta. The discovery of these dust grains offers an indirect evidence for the dust formation and growth in the CE ejecta. Therefore, CE ejecta is an efficient dust source. However, to our knowledge, there is no work considering CE ejecta as dust source on estimating dust budget in the LMC.

In this work, we investigate the contributions of dust formed by CE ejecta to the interstellar dust, and give a new dust budget in the LMC. In §2 the model of the ejecta during binary merger is described. The main results and discussions are presented in §3. §4 gives conclusions.

## 2 MODEL

Before discussing dust formation and growth in CE ejecta, we give some descriptions for CE and CE ejecta evolution, and the chemical abundances of CE ejecta.

### 2.1 Common Envelope Evolution

As a result of dynamical timescale mass exchange in close binaries, CE evolution plays an essential role in binary evolutions (see, e.g., Paczynski 1976; Iben & Livio 1993). Unfortunately, based on observation data and theoretical models, CE evolution is poorly known. In this work, we adopt the scheme by Hurley et al. (2002) to simulate CE evolution. All details can be seen in Section 2 of Hurley et al. (2002). In most cases, CE evolution involves a giant star (donor) transferring matter to a normal or a degenerate star (gainer) on a dynamical timescale. If the orbital energy of the binary system is large enough, the whole envelope of the gainer is ejected as CE ejecta.

### 2.2 The Evolutions of Gas Density and Temperature in CE Ejecta

When CE ejecta begins to expand, its temperature and mass density start to decrease. According to the classical theory of nucleation (Feder et al. 1966), in most cases the formation of dust grains can occur in adiabatically expanding gas, and is mainly determined by temperature, mass density and chemistry of the gas phase. In order to simulate the dust formation and growth in CE ejecta, we must determine the evolutions of gas density and temperature. To our knowledge, there is no any comprehensive theoretical model or observational datum to describe the mass density and the temperature of CE ejecta.

Considering the whole envelope is ejected on a dynamical timescale during CE evolution, we assume that initial temperature ( $T_0$ ) and density ( $\rho_0$ ) of CE ejecta are equal to the temperature and the mass density of stellar matter in the giant envelope, respectively. In this work, the stellar structure and evolution are simulated via a stellar evolution code developed by Eggleton (1971, 1972) and Eggleton et al. (1973), which has been updated with the latest input physics over the past three decades (e. g., Han et al. 1994). The giant envelope refers to the region in which the hydrogen abundance (by mass) is larger than 0.5. When CE evolution occurs, the giant envelope is ejected, shell by shell. Each shell expands outwards with no overlapping between shells. The  $T_0$  and  $\rho_0$  of each shell are given by the stellar evolution code, and their evolutions are described in the following two paragraphs.

We assume that the CE ejecta is an adiabatically expanding perfect gas. The mass density,  $\rho$ , is given by

$$\rho = \dot{M}_{\text{ej}} / (4\pi R^2 V), \quad (1)$$

where  $\dot{M}_{\text{ej}}$ ,  $R$  and  $V$  are the mass-ejection rate, the radial distance of the ejected matter and the velocity of the ejected matter. Some numerical simulations for CE evolution give  $V \sim 100 \text{ km s}^{-1}$ , which is close to the local escape velocity (e. g., Kashi & Soker 2011). In this work, we assume that

$$V \simeq V_{\text{esc}} = \sqrt{\frac{2GM}{R}}, \quad (2)$$

where  $G$  is the gravitational constant and  $M$  is the stellar mass. However, considering the conservation of mass during CE expansion, we obtain

$$\dot{M}_{\text{ej}} = \rho 4\pi R^2 V = \rho_0 4\pi R_0^2 V_0, \quad (3)$$

where  $R_0$  is the initial distance of a given shell of the envelope from the stellar center. Here,  $V_0 = \sqrt{\frac{2GM}{R_0}}$ . The gas density of the same shell at a distance  $R$  from the donor center is given by

$$\rho = \rho_0(R/R_0)^{-3/2}. \quad (4)$$

For an adiabatically expanding perfect gas,  $\rho T^{\frac{1}{1-\gamma_{\text{ad}}}} = \text{constant}$ . Based on the results of model calculations in Fransson & Chevalier (1989), Kozasa et al. (1989) adopted an adiabatic index  $\gamma_{\text{ad}}$  as 1.25 for the early stage of SN explosion. In this work, we also take  $\gamma_{\text{ad}}$  as 1.25. Therefore, the temperature of the shell at  $R$  from the donor center is calculated by

$$T = T_0 \left( \frac{R}{R_0} \right)^{-0.375}. \quad (5)$$

Eqs. (1)–(5) determine the evolution of mass density and temperature of every shell in CE ejecta.

### 2.3 Chemical Abundances of CE Ejecta

The chemical abundances of CE ejecta are determined by the donor's envelope. For a single star, three dredge-up processes and hot bottom burning (the latter only in a star with initial mass higher than  $4M_{\odot}$ ) may change the chemical abundances of the stellar envelope. During each dredge-up event the base of the convective envelope extends inwards to shells previously involved in nuclear burning and nuclearly processed matter is transported to the external zones of the star (e. g., Iben & Renzini 1983; Herwig 2005). The first dredge-up occurs during the first ascent of the giant branch (FGB). Sufficiently massive stars ( $M_i > 4M_{\odot}$ ) undergo the second dredge-up after the end of He-core burning (e. g., Herwig 2005). The third dredge-up occurs when the stars evolve to thermal pulse AGB (TPAGB) phase. If the mass of the hydrogen envelope above the He-exhausted core is large enough and the core mass is above  $\sim 0.8M_{\odot}$ , the hydrogen burning shell can extend into the bottom of the convective region, which is called as hot bottom burning. Reviews about dredge-ups and hot bottom burning were given by Iben & Renzini (1983) and Herwig (2005).

As discussed in the previous section, we use Eggleton's code to simulate the evolution of a star from the premain sequence to the end of the AGB phase. However, this code does not simulate the effects of third dredge-up process and hot bottom burning on the chemistry of stellar envelope. In this work, we use the model of Lü et al. (2008) to simulate the chemical evolutions of  $^1\text{H}$ ,  $^4\text{He}$ ,  $^{12}\text{C}$ ,  $^{13}\text{C}$ ,  $^{14}\text{N}$ ,  $^{15}\text{N}$ ,  $^{16}\text{O}$ ,  $^{17}\text{O}$ ,  $^{20}\text{Ne}$  and  $^{22}\text{Ne}$  in the stellar envelope. Lü et al. (2008) followed the prescriptions by Izzard et al. (2004) for the first dredge-up during FGB and the second dredge-up during early AGB. For the third dredge-up and the hot bottom burning during the TPAGB phase, we use the TPAGB synthesis in Groenewegen & de Jong (1993), Karakas et al. (2002), Izzard et al. (2004) and Marigo & Girardi (2007). All details can be found in Appendix A of Lü et al. (2008).

Mass transfer in a binary system can change the chemical abundances of the stellar envelope. In binary systems, there are two ways to transfer mass: (i) accretion from the stellar wind material of a companion star; (ii) Roche lobe overflow. After the gainer in a binary system obtains

mass ( $\Delta M$ ) from the donor, the chemical abundances of the stellar surface,  $X_g$ , are given by

$$X_g^{\text{new}} = \frac{X_g^{\text{old}} \times M_g^{\text{env}} + X_d \times \Delta M}{M_g^{\text{env}} + \Delta M}, \quad (6)$$

where  $M^{\text{env}}$  is the envelope mass and  $X$  is the chemical abundances of its companion star, g and d indicate the gainer and the donor in a binary system, respectively.

Then, we follow the chemical evolutions of  $^1\text{H}$ ,  $^4\text{He}$ ,  $^{12}\text{C}$ ,  $^{13}\text{C}$ ,  $^{14}\text{N}$ ,  $^{15}\text{N}$ ,  $^{16}\text{O}$ ,  $^{17}\text{O}$ ,  $^{20}\text{Ne}$  and  $^{22}\text{Ne}$  in the stellar envelope of binary system. The abundance ratio of carbon to oxygen,  $C/O = (^{12}\text{C} + ^{13}\text{C})/(^{16}\text{O} + ^{17}\text{O})$ , determines the dust species produced by CE ejecta. O-rich ejecta ( $C/O < 1$ ) forms silicate dust, while C-rich ejecta ( $C/O > 1$ ) produce amorphous carbon and SiC. Following Ferrarotti & Gail (2006), we assume that the abundances of other key elements (Fe, Si, Mg and S) for the dust formation do not change.

Following Lü et al. (2008), we use a synthetic stellar evolution model to calculate the evolution of chemical abundances. Figure 1 shows the time evolution of the surface  $C/O$  of stars with different masses. The evolutions of  $C/O$  mainly depend on the initial masses of the stars:

- (1) All stars undergo the first dredge-up during the FGB phase. Its effects mainly are that carbon abundance on the stellar surface is reduced by approximately 30% and oxygen abundance does not change. As Figure 1 shows,  $C/O$ s of all stars decrease after the first dredge-up. The second dredge-up, occurring in models with mass above  $4M_{\odot}$ , hardly changes the  $C/O$  ratio (e. g., Izzard et al. 2004).
- (2) Low-mass stars ( $M < 1.5M_{\odot}$ ) never become carbon stars, owing to the small number of thermal pulses experienced.
- (3) Stars with initial masses between about  $1.5 M_{\odot}$  and  $4.0 M_{\odot}$  increase their carbon abundance over the oxygen abundance after a number of thermal pulses. The surface  $C/O$  soon exceeds unity.
- (4) Intermediate mass stars with initial masses between about  $4 M_{\odot}$  and  $8 M_{\odot}$  convert the dredged-up carbon rapidly into  $^{14}\text{N}$  via the CN-cycle due to hot bottom burning. However, the oxygen is not affected by this process. Therefore, the carbon abundance in the envelopes of these stars is much less than the oxygen abundance. These stars never become carbon stars.

### 2.4 Dust Formation and Growth in CE Ejecta

With the decrease of CE ejecta's temperature due to its expansion, dust can form and grow. In this work, with the help of *AGBDUST* code (kindly provided by Prof. Gail, private communication), we replace the thermodynamic structure of the wind from AGB star in the *AGBDUST* code with Eqs. (4) and (5), and use the model of formation and growth of dust grains in the *AGBDUST* code to simulate the formation and growth of dust grains in CE ejecta.

The model of formation and growth of dust grains in the *AGBDUST* code assumes that the dust grains grow on some kinds of seed nuclei. The seed nuclei are formed prior to the point where the different dust components start to condense. The radii of these seed nuclei are denoted by  $a_0$ . The *AGBDUST* code assumes  $a_0 = 1$  nm for the radii of the seed nuclei. If the wind is accelerated by radiation pressure,

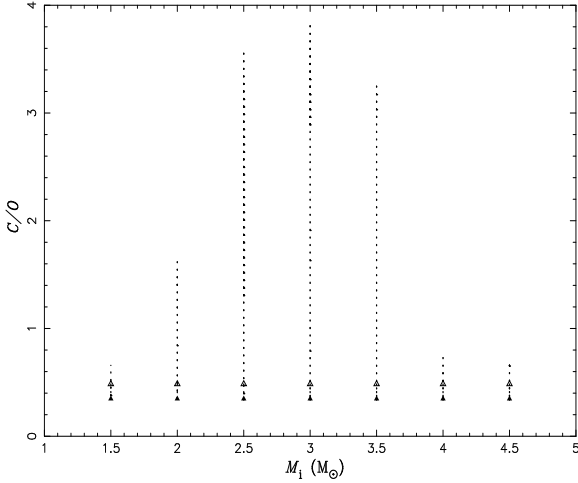


**Figure 1.** The evolutions of  $C/O$ s in the stellar envelopes with different initial masses. The dotted lines represent the evolutions of  $C/O$ s. The empty and solid triangles give the initial  $C/O$ s and the  $C/O$ s after stars undergo the first dredge-up (FDU), respectively. The tops of dotted lines represent the maximum values of  $C/O$ s at the end of AGB phase.

the final results for the grain radii are nearly independent of the particular assumption on  $a_0$ . Then, the growth of the grain size of species  $i$  is calculated via the equation

$$\frac{da_i}{dt} = V_{0,i}(J_i^{\text{gr}} - J_i^{\text{dec}}), \quad (7)$$

where  $a_i$  is the radius of dust species  $i$ , and  $V_{0,i}$  is the volume of the nominal molecule in the solid. Here,  $J_i^{\text{gr}}$  is the deposition rate per unit time and surface area for a particle in rest with respect to the gas phase. It is given by

$$J_i^{\text{gr}} = \alpha_i n_i v_{\text{th},i}, \quad (8)$$

where  $\alpha_i$  denotes the sticking coefficient,  $n_i$  gives the particle density in the gas phase and  $v_{\text{th},i} = \sqrt{\frac{kT}{2m_i}}$  is the mean thermal velocity of the particles. Here,  $k$  is the Boltzmann constant and  $T$  is the temperature. The  $J_i^{\text{dec}}$  is decomposition rate in a thermodynamic equilibrium state, which is given by

$$J_i^{\text{dec}} = \alpha_i v_{\text{th},i} \frac{p_i}{kT}, \quad (9)$$

where  $p_i$  is the partial pressure of the molecules of dust species  $i$  in chemical equilibrium between the gas phase and the solid phase.

The amount of dust formed is indicated by the fraction of gas condensed into solid grains, i.e. the degree of condensation (Gail & Sedlmayr 1999). For each species, the *AGBDUST* code selects a key-element  $k$ . Its degree of condensation is expressed by,  $f_k^i$ , the fraction of the key-element in dust species  $i$ , which is given by

$$f_k^i = \frac{4\pi[(a_i)^3 - (a_0)^3]}{3V_{0,i}} \frac{n_{\text{d},i}}{\epsilon_k N_{\text{H}}}, \quad (10)$$

where  $n_{\text{d},i}$  is the number density of seed nuclei of the different dust species,  $\epsilon_k$  is the key-element abundance by number relative to H abundance, and  $N_{\text{H}}$  is the number density of hydrogen nuclei. In the *AGBDUST* code,  $n_{\text{d},i} = 3 \times 10^{-13} N_{\text{H}}$  for all dust species (Ferrarotti & Gail 2003).

Based on the degrees of condensation of key-element ( $f_k^i$ ) in dust species  $i$ , the DPR in CE ejecta is calculated by

$$\frac{dM_{\text{d}}^i}{dt} = \dot{M}_{\text{ej}} X_k \frac{A_i}{A_k} f_k^i, \quad (11)$$

where  $X_k$  is the key-element abundance in CE ejecta by mass,  $A_i$  and  $A_k$  are the molecular and atomic weights of the dust species  $i$  and the key-element  $k$ , respectively.

Table 1 gives a list of the dust species considered in the present paper, their formation reactions, the corresponding key-elements and the sticking coefficient ( $\alpha_i$ ). The thermodynamic quantities (mainly the free energies used to calculate the equilibrium pressures) of the reactions are taken from Sharp & Huebner (1990). The composition of olivine and pyroxene depends on the relative fraction of magnesium and iron, indicated, with  $x$  and  $1 - x$  (see Table 1), respectively. The details for calculating the magnesium percentages in the olivine and pyroxene dust grains can be found in Gail & Sedlmayr (1999). To our knowledge, there is not experimentally determined data for the sticking coefficient. We adopt the values of  $\alpha_i$  in Ferrarotti & Gail (2003) which are mainly based on Hashimoto (1990) and Nagahara & Ozawa (1996).

### 3 DUST YIELDS FROM CE EJECTA

Based on the model of dust formation and growth in CE ejecta described in the last section, dust yields not only depend on the parameters listed in Table 1, but also on the initial temperature ( $T_0$ ) and density ( $\rho_0$ ), the chemical abundances (mainly  $C/O$ ) and the mass of CE ejecta.

In this section, we take  $Z = 0.008$  as an example to calculate the dust yields from CE ejecta. The initial abundances of all heavy elements are approximately equal to 0.4 times those of the Sun. The element abundances on the surface of the Sun are taken from Anders & Grevesse (1989).

#### 3.1 Typical Examples

As discussed in §2, CE evolution involves a giant or giant-like envelope. This giant star may evolve in the Hertzsprung gap (HZ), FGB or AGB. The envelopes at different evolutionary stages have different structures (mass density, temperature and chemical abundances), which may affect the dust formation and growth in the CE ejecta. In order to discuss these effects, we select two groups of typical examples: one is that CE ejecta originate from an envelope of a star with initial mass of  $1M_{\odot}$  at the beginning of HZ, the beginning of FGB, the end of FGB, the beginning of AGB and TPAGB, respectively; the other is that CE ejecta is produced by an envelope of a star with initial mass of  $3M_{\odot}$  at the begin of HZ, the begin of FGB, the end of FGB, the begin of AGB, and  $C/O = 2$  at TPAGB due to the third dredge-up, respectively.

Figure 2 shows the initial temperature and density profiles of the giant envelopes as a function of relative mass coordinate for the two groups of typical examples. The external regions of the stars expand during the evolution, with the consequent decrease of temperature and density. The mass of the envelope diminishes, owing to mass loss.

**Table 1.** Dust species considered in the present paper, their formation reactions, the corresponding key-elements, and the sticking coefficient ( $\alpha_i$ ).

Dust Species	Formation Reactions	Key-Elements	$\alpha_i$
Olivine	$2x\text{Mg} + 2(1-x)\text{Fe} + \text{SiO} + 3\text{H}_2\text{O} \rightarrow \text{Mg}_{2x}\text{Fe}_{2(1-x)}\text{SiO}_4 + 3\text{H}_2$	Si	0.15
Pyroxene	$x\text{Mg} + (1-x)\text{Fe} + \text{SiO} + 2\text{H}_2\text{O} \rightarrow \text{Mg}_x\text{Fe}_{(1-x)}\text{SiO}_3 + 2\text{H}_2$	Si	0.15
Quartz	$\text{SiO} + \text{H}_2\text{O} \rightarrow \text{SiO}_2(\text{s}) + \text{H}_2$	Si	0.1
Silicon Carbide	$2\text{Si} + \text{C}_2\text{H}_2 \rightarrow 2\text{SiC} + \text{H}_2$	Si	0.3
Carbon	$\text{C} \rightarrow \text{C}(\text{s})$	C	0.3
Iron	$\text{Fe} \rightarrow \text{Fe}(\text{s})$	Fe	0.8

As shown in Figure 2, at the beginning of CE expansion the temperatures in the envelope are too large (higher than  $\sim 10^4$  K) to allow dust formation. During the expansion the CE ejecta reach regions  $10^{13}$ – $10^{16}$  cm away from the donor, where the temperatures are below 2000K, thus rendering possible condensation of gas molecules into dust (Lü et al. 2013). By means of the *AGBDUST* code we simulate dust formation and growth within the expanding envelope. The computation is run for each shell, of initial temperature  $T_0$ , into which the envelope is divided. Figures 3 and 4 show the condensation degrees of key elements and the mass of dust formed in the expanding shells of the envelope of two stars of mass 1 and 3 solar masses.

The dust formation and growth in CE ejecta has its own features:

(i) High condensation degrees. The main reason is that the dust-forming zones in the CE ejecta ( $T < \sim 1300$  K) have very high mass density ( $\sim 3.3 \times 10^{-11} \text{ g cm}^{-3}$ ). Based on Eqs.(7) and (8), the higher is the mass density, the higher is the growth rate of grain size, which results in a high condensate degree. For AGB wind with a high mass-loss rate of  $1 \times 10^{-5} M_\odot \text{ yr}^{-1}$  and a wind structure based on Ferrarotti & Gail (2006), *AGBDUST* code shows that the temperature and the mass density of dust-forming zones are  $\sim 1.3 \times 10^3$  K and  $5.0 \times 10^{-14} \text{ g cm}^{-3}$ , respectively. About 32% of Si atoms in AGB wind condensate into silicates, and about 4% of Fe atoms condensate into iron grains. However, in our simulations, all of Si and Fe atoms in CE ejecta condensate into silicate ( $f_{\text{OL}} + f_{\text{QU}} + f_{\text{PY}} \sim 1$ ) and iron grains ( $f_{\text{IR}} \sim 1$ ), respectively.

(ii) Silicate grains are mainly made up of pure forsterite ( $\text{Mg}_2\text{SiO}_4$ ) and quartz grains. At the region of dust formation and growth, compared with AGB stellar wind, CE ejecta has higher temperature and mass density. Based on the stability limits of some grains and molecules (See Fig. 2 in Gail & Sedlmayr (1999)), forsterite, iron and quartz grains firstly form. Most of Fe atoms condensate into iron grains. Therefore, olivine-type ( $\text{Mg}_{2x}\text{Fe}_{2(1-x)}\text{SiO}_4$ ) grains are mainly made up of pure forsterite ( $\text{Mg}_2\text{SiO}_4$ ) grains.

As Figures 3 and 4 show, almost all of Fe atoms in CE ejecta condensate into iron grains. In a CE ejecta ( $C/O < 1$ ), most of Si element condensates into silicate grains; In CE ejecta ( $C/O > 1$ ), a part of C atoms and most of O atoms combine CO molecule, while most of left C atoms condensate into carbon grains. Therefore, CE ejecta can efficiently produce dust grains, and the dust mass mainly depends on the mass of CE ejecta.

### 3.2 Comparison with AGB Stars

AGB stars, as important stellar sources of dust, have been investigated by many independent groups. Having used synthetic stellar evolution models, Zhukovska et al. (2008) computed dust condensation and estimated the dust yields for M, S, and C-type AGB stars of different ages and metallicities. Based on these models, Zhukovska & Henning (2013) estimated dust input from AGB stars in the LMC. However, as Schneider et al. (2014) pointed out, their major drawback was that they used simple evolutionary code based on analytic approximations to describe complex physical processes, primarily third dredge-up and hot bottom burning. These processes directly affect the chemical abundances and physical conditions in AGB envelope, thus they determine the dust yields. Ventura and collaborators used the ATON code to produce accurate modelling of the AGB phase and computed the mass and composition of dust produced by AGB stars (Ventura et al. (2012); Ventura et al. (2012); Di Criscienzo et al. (2013)). Following Schneider et al. (2014), we call this code as old ATON. Zhukovska & Henning (2013) found that, compared with observations, the old ATON yields underestimated the dust production rate from C-rich AGB stars. For this reason, Ventura et al. (2014) calculated new AGB evolutionary sequences with a deeper third dredge-up, and Schneider et al. (2014) provided new dust yields, to which we refer to as new ATON. However, there are some differences of dust mass and composition among Zhukovska et al. (2008), old and new ATON. Detailed reasons had been discussed by Schneider et al. (2014) and Ventura et al. (2014).

As discussed in next section, based on the observational data, several investigations estimated the DPRs from AGB stars in the LMC, and their results have large scatter. By comparing the observed and predicted DPRs of the Magellanic Clouds, Schneider et al. (2014) found that old ATON models are better suited for  $Z \leq 0.004$ , while use of the new ATON models is recommended for  $Z = 0.008$ . In this work, in order to compare the dust yields produced by CE ejecta with those by AGB stars, we use the above three models.

In Figure 5, we compare the dust masses of different compositions from CE ejecta formed at different evolutionary stages with those from AGB stars by Zhukovska et al. (2008), old and new ATON. Due to the high condensation degrees in almost the whole envelope, CE ejecta produces more efficiently silicate and iron grains. In our model, the stars with initial masses between  $\sim 1.5$  and  $4.0 M_\odot$  evolve to carbon stars and produce carbon and SiC grains, similar to the results of old and new ATON. On the other hand, having used a model for TPAGB with efficient third dredge-

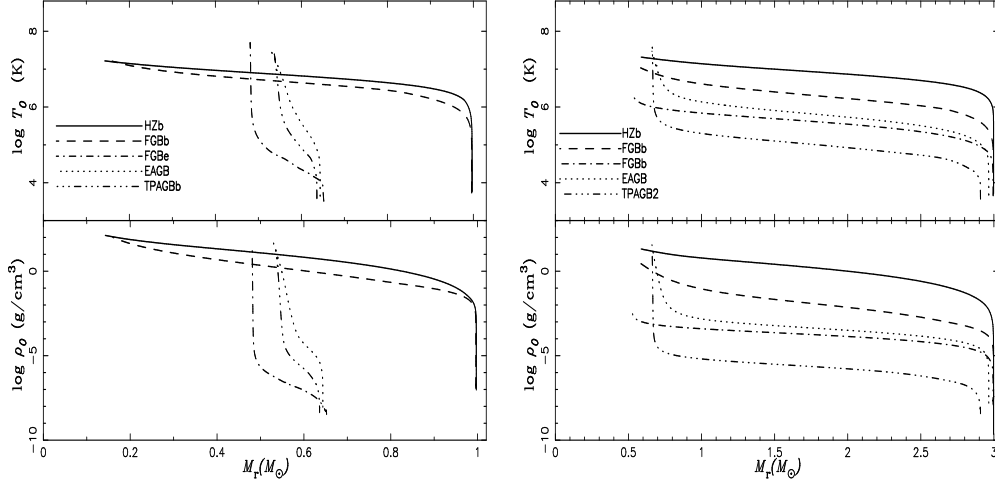


**Figure 2.** The initial temperature and density profiles of the envelopes of giants (at different evolutionary stages as indicated) as a function of relative mass coordinate. 'HZb', 'FGBb', 'FGBc', 'EAGB' and 'TPAGBb' mean that star just evolves at the begin of Hertzsprung gap, the begin of the FGB, the end of the FGB, the begin of the AGB and the begin of the thermally pulsing AGB (TPAGB), respectively. 'TPAGB2' means that  $C/O$  of stellar envelope increases to 2.0 because of the third dredge-up. The left and right panels are for the star with mass of 1 and  $3 M_{\odot}$  at zero-age main sequence, respectively.

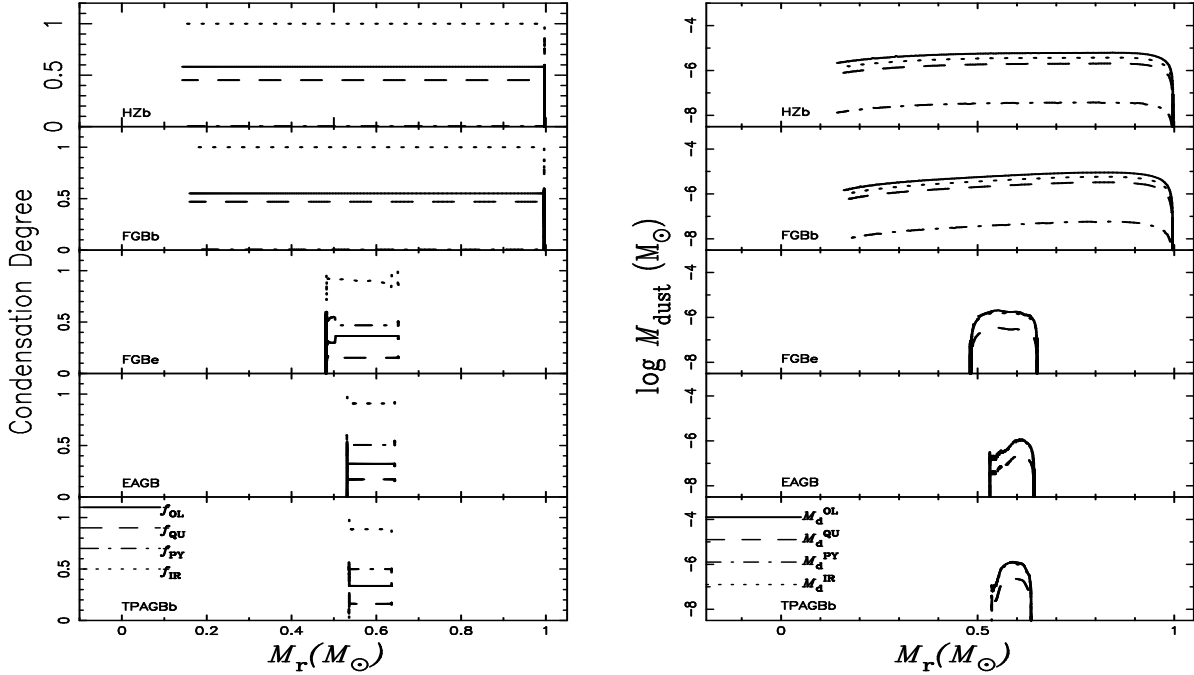


**Figure 3.** Condensation degrees of key-elements and dust yields of different dust species as a function of relative mass coordinate at different evolutionary stages for the star with mass of  $1 M_{\odot}$  when stellar envelope is ejected into a region where dust can form and grow (Details in text). The ' $f_{OL}$ ', ' $f_{QU}$ ' and ' $f_{PY}$ ' present the condensation degrees of Si element in olivine-type, pyroxene-type and quartz grains, respectively. The ' $f_{IR}$ ' means the condensation degree of Fe element in iron grains. Correspondingly, the ' $M_d$ 's present the dust yields of different dust species.

up and weak hot bottom burning, the stars between  $\sim 1$  and  $8 M_{\odot}$  in Zhukovska et al. (2008) can become carbon stars with high  $C/O$  at the end of AGB stars. Therefore, their models produced more carbon grains and less silicates.

### 3.3 Comparison with Supernova

SNe II are considered as another important stellar sources of dust. Due to their short lifetimes and large production of metals, they are regarded as the most likely sources of dust in high red-shift galaxies and quasars (e.g., Dwek 1998; Gall et al. 2011). Unfortunately, no matter observations or theoretical models, there is no reliable result to definitively calculate which species of dust formed and in



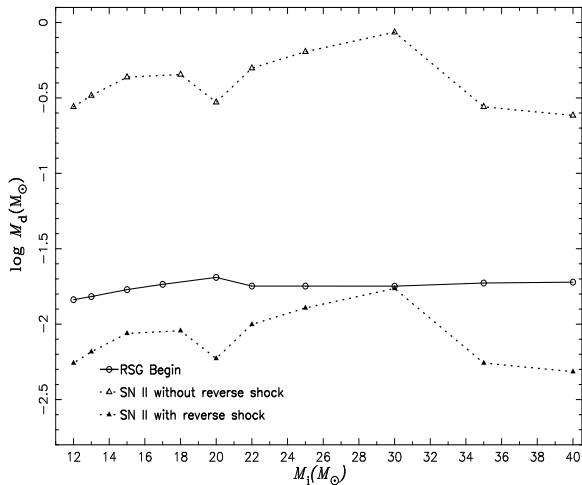


**Figure 6.** Comparison of the dust yields from CE ejecta formed by massive stars at the begin of red supergiant (RSG). The dust yields from SNe II without reverse shock come from Todini & Ferrara (2001). The dust yields from SNe II with reverse shock mean that only about 2 percent of dust mass survive after reverse shock.

passage of the reverse shock, depending on the density of the surrounding interstellar medium.

In a binary system, if a massive star fills its Roche lobe when it evolves into the red supergiant (RSG) state, its envelope can also be ejected as CE ejecta. We compare in Figure 6 the dust yields in CE ejecta with those from SNe II. In the ejecta of SNe II, there is a large quantity of metal elements. In the model of Todini & Ferrara (2001), most of them condensate into dust grains. Therefore, compared with the ejecta of SNe II without dust destruction, dust produced by CE ejecta from massive star is negligible. However, as Bianchi & Schneider (2007) showed, most of dust produced by the ejecta of SNe II are soon destroyed by reverse shock. If only about 2 percent of the initial dust mass produced by the ejecta of SNe II can survive after the reverse shock, dust produced by CE ejecta from massive star is dominant.

## 4 DUST BUDGET IN THE LMC

As shown in the last section, AGB stars, the ejecta from SNe II and CE are potential sources of dust in the LMC. In order to calculate their contributions to total dust in the LMC, we use a method of population synthesis.

### 4.1 Basic Parameters of Population Synthesis

For a method of population synthesis, the main input parameters are: (i) the initial mass function (IMF); (ii) the mass-ratio distribution for binaries; (iii) the eccentricity distribution for binaries; (iv) the distribution of orbital separations for binaries. We use a Salpeter initial mass-function for single stars and primary components in binaries:

$$\phi(m) = Cm^{-2.35}, \quad (12)$$

with normalisation number  $C = 0.06$  within the mass integral range between 0.1 and  $100 M_{\odot}$ . For binary systems, we must know the distribution of the ratios of components.

Based on Kraicheva et al. (1989) and Goldberg & Mazeh (1994), a flat distribution of initial mass ratios of components is assumed in this work. Meanwhile we assume that all binaries have initially circular orbits. In our work, one of the most important input parameters is the distribution of initial binary separations which directly determine how many binaries undergo Roche-lobe overflow. However, to our knowledge, there is no any confirmed observational evidence to describe it. Eldridge et al. (2008) assumed that a flat distribution over  $1 < \log a_0/R_{\odot} < 4$  (also see Tout et al. 2014), where  $a_0$  is the initial binary separation. In this work, we adopt the above distribution.

### 4.2 Star Formation Rate

The dust quantities in the LMC depend on the star formation rate (SFR). According to the Magellanic Clouds Photometric Survey including 20 million LMC stars and using the StarFISH analysis software, Harris & Zaritsky (2009) reconstructed the SFR of the LMC during different ages. Harris & Zaritsky (2009) found that the optimal solution includes the four metallicities  $Z = 0.001, 0.0025, 0.004, 0.008$ . The separate contributions of the four metallicities during different ages are shown in Figure 7. Since we are interested in the dust quantities of the whole LMC, we average over SFRs of individual regions for each age bin.

### 4.3 Initial Binary Fraction in the LMC

In our work, dust formation involves binary systems. Therefore, the binary fraction in all stars of the LMC is very important. There is no observational evidence to help us in adopting a binary fraction. Harris & Zaritsky (2009) simply assumed that the binary fraction in the LMC is 50%. However, it does not give solid information for the initial binary fraction. According to the theoretical model of binary evolution, binary systems can become single stars if they undergo binary merger or they are disrupted by supernovae. For example, for binary systems whose initial conditions are given in §4.1, about 38% of binaries do not undergo Roche lobe mass transfer, and their evolutions are similar to single stars. About 62% of binaries undergo Roche lobe overflow at least once, in which about 73% undergo CE evolution and can eject the whole CE at least once, while about 27% can not eject the CE and usually merge into single stars. In short, about 54% of these binary systems may be observed as single stars.

In this work, in order to check the effects of initial binary fraction on the dust budget in the LMC, we use two different initial binary fractions: one is an initial binary fraction of 50% (a half of SFR in the LMC is for binary systems and another half is for single stars), the other is that the initial binary fraction is 100%, that is, all stars are born in binary systems.

### 4.4 Calculation of Dust Production Rates

Using IMF, SFR and dust yields discussed in the previous sections, we can theoretically calculate DPRs from the above three sources in the LMC.

For a single star, following Zhukovska & Henning



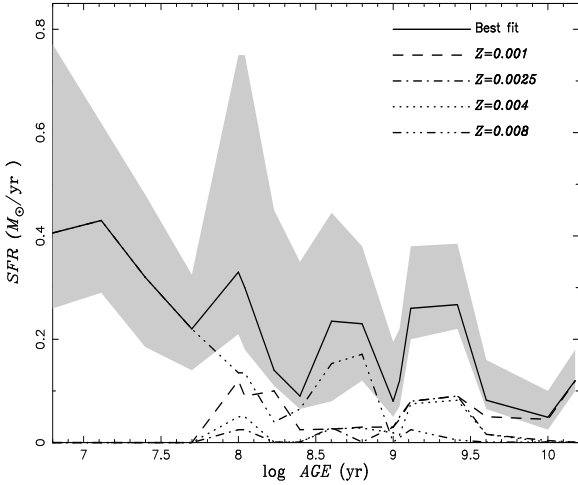


**Figure 7.** Star formation history in the LMC with the age from Harris & Zaritsky (2009). The best-fit SFR as a function of age is showed with a solid line, and the uncertainty on the fit is showed as an oblique-line area. Dashed, dash-dotted, dotted, dash-dot-dotted lines present the contributions of  $Z = 0.001$ ,  $0.0025$ ,  $0.004$  and  $0.008$ , respectively.

(2013) and Schneider et al. (2014), the DPRs of the type  $j$  dust grains from AGB stars at time  $t$  can be estimated by

$$\dot{M}_d^j = \int_{m_L}^{m_U} \phi(m) \frac{SFR(t - \tau(m, Z))}{2} m_d^j(m, Z) dm, \quad (13)$$

where  $\phi(m)$  is IMF,  $SFR(t - \tau(m, Z))$  is SFR,  $\tau(m, Z)$  is the lifetime of a star with mass  $m$  and metallicity  $Z$  when it leaves AGB stage, and  $m_d^j(m, Z)$  is the mass of dust. The lower integration limit,  $m_L$ , is determined by a stellar mass with the lifetime which satisfies  $\tau(m_L) = t$ , and the upper mass-limit  $m_U = 8M_\odot$  is determined by stars becoming AGB stars. The  $m_d^j(m, Z)$  can be obtained by the linear interpolation in a given grid of dust yields from Zhukovska et al. (2008) or Schneider et al. (2014). Similarly, the DPRs of the type  $j$  dust grains from SNe II at time  $t$  can also be calculated by Eq.(13), but the upper mass-limit  $m_U = 40M_\odot$  and the  $m_d^j(m, Z)$  can be obtained from Todini & Ferrara (2001).

For a binary system in which the initial masses of primary and secondary are  $m_1$  and  $m_2$  and the initial binary separation is  $a_0$ , the DPR of the type  $j$  dust grains from CE ejecta at time  $t$  can be estimated by

$$\dot{M}_d^j = \int_{m_L}^{m_U} \phi(m_1) \int_{m_L}^{m_1} \phi(m_2) \int_{10^4}^{10^5} \varphi(a_0) \frac{SFR(t - \tau(m_1, m_2, a_0))}{2} m_d^j(m_1, m_2, a_0) dm_1 dm_2 da_0, \quad (14)$$

where  $\tau(m_1, m_2, a_0)$  is the time of a binary system occurring CE evolution, and  $m_d^j(m_1, m_2, a_0)$  is dust mass produced by CE ejecta. In order to calculate  $m_d^j(m_1, m_2, a_0)$ , for the four metallicities ( $Z = 0.001, 0.0025, 0.004, 0.008$ ), we calculate dust yields which are for different stellar masses ( $m = 1.0, 1.5, 2.0, 2.5, 3.0, 3.5, 4.0, 4.5, 5.0, 5.5, 6.0, 8.0M_\odot$ ) in different evolutionary phases (HZ, the beginning of FGB, the end of FGB, the beginning of AGB and TPAGB). We do not consider massive stars due to mass function. When a binary system undergoes CE evolution, by the linear interpolation of the donor's mass and age in the dust yields, we obtain  $m_d^j(m_1, m_2, a_0)$ .

#### 4.5 Dust Production Rates

Based on observational data of a number of surveys, DPRs from C-rich and O-rich AGB stars in the LMC had been estimated by Matsuura et al. (2009), Srinivasan et al. (2009), Boyer et al. (2012) and Riebel et al. (2012). Unfortunately, as Figure 8 shows, there is a large scatter between the above observationally estimated DPRs. DPRs from C-rich AGB stars estimated by Matsuura et al. (2009) are larger than  $4.3 \times 10^{-5} M_\odot \text{ yr}^{-1}$  (up to  $1.0 \times 10^{-4} M_\odot \text{ yr}^{-1}$ ), while they are  $2.4 \times 10^{-6} M_\odot \text{ yr}^{-1}$  in Srinivasan et al. (2009),  $8.7 \times 10^{-7} M_\odot \text{ yr}^{-1}$  in Boyer et al. (2012),  $5.2\text{--}5.7 \times 10^{-6} M_\odot \text{ yr}^{-1}$  in Riebel et al. (2012), respectively. Similar scatter appears in DPRs from O-rich AGB stars. Differences of the DPRs observationally estimated mainly result from various approaches and source classifications (Details can be seen in Zhukovska & Henning (2013)).

Similarly, there is also a large difference between the theoretically estimated DPRs. Using the dust yields of AGB stars in Zhukovska et al. (2008), Zhukovska & Henning (2013) predicted that the DPRs from C-rich and O-rich AGB stars in the LMC are  $5.7 \times 10^{-5} M_\odot \text{ yr}^{-1}$  and  $1.3 \times 10^{-6} M_\odot \text{ yr}^{-1}$ , respectively. However, using the dust yields of AGB stars from old ATON, Zhukovska & Henning (2013) calculated that they were  $6.3 \times 10^{-6} M_\odot \text{ yr}^{-1}$  and  $1.1 \times 10^{-5} M_\odot \text{ yr}^{-1}$ , respectively. The uncertainty introduced by different models for AGB stars is up to about 10. Using the dust yields of AGB stars from Zhukovska et al. (2008), old and new ATON, Schneider et al. (2014) also predicted the DPRs in the LMC. They found that the DPR from C-rich AGB stars calculated by the dust yields of AGB stars from Zhukovska et al. (2008) is close to that calculated by new ATON, while the DPR from O-rich AGB stars by new ATON is close to that by old ATON. The main reason behind these differences is in the treatment of convective borders and in the efficiency of the convective models used, that affect the extent of the third dredge-up and the strength of hot bottom burning (Details can be seen in Schneider et al. (2014)). However, to our knowledge, all theoretical estimates did not consider the effect of binary interaction on the DPRs in the LMC. In this work we compare the DPRs of AGB stars in the LMC with those from Zhukovska et al. (2008), old and new ATON. Simultaneously, we also estimates the DPRs of CE ejecta in the LMC. As Figure 8 shows, the initial binary fraction changing from 50% to 100% introduces an uncertainty of a factor of about 1.5 — 2 to the DPRs from AGB stars and from CE ejecta, respectively. These uncertainties are much smaller than these differences between different observational or theoretical estimates.

Due to large scatters between observationally estimated or theoretically predicted DPRs from AGB stars, we can not determine whether the DPRs from CE ejecta are significant. However, we find that CE ejecta can efficiently produce silicate and iron grains, while carbon grains are negligible. The main reason is that in our models most of CE events occur before the third dredge-up works efficiently.

In order to compare the contributions of different sources to the DPRs in the LMC, Figure 9 shows the total DPRs from CE ejecta, AGB star and SNe II with the age of the LMC by using the best-fit star formation histories. If we do not consider the destruction by reverse

shock, the majority of dust grains in the LMC originate from SNe II. However, if only 2% of dust grains can survive after reverse shock, compared with AGB stars calculated by Zhukovska et al. (2008) and new ATON, the contribution of SNe II to the total DPRs is negligible. In the simulation with an initial binary fraction of 50%, the DPR from CE ejecta is close to that calculated by old ATON, but it is only 1/4 of those calculated by Zhukovska et al. (2008) and new ATON. However, it is about 4 times of the former and about 3/4 times of the latter in the simulation with an initial binary fraction of 100%. One should take note that the assumption of 100% binary fraction is realistic. Here, we only want to estimate an upper limit of the DPR from CE ejecta. More importantly, most of dust grains calculated by Zhukovska et al. (2008) and new ATON are carbon. Formation of C-rich AGB stars deeply depend on a complex physical process: the third dredge-up. In new ATON model and Zhukovska et al. (2008), the third dredge-up is more efficient, and C-rich AGB stars form more easily. However, in old ATON, it is difficult for a star to evolve into C-rich AGB star, and the DPR from C-rich AGB stars in the LMC is negligible (Zhukovska et al. 2008; Schneider et al. 2014).

In short, although the DPRs in the LMC estimated by observational data or theoretical models are very uncertain, we consider that the contributions of CE ejecta must be included when the total DPRs in the LMC are calculated.

#### 4.6 Total Dust Budget

The total dust mass,  $M_{\text{dust}}$ , is very important for understanding the dust formation, evolution and destruction in the LMC. Therefore, there are many literatures to estimate  $M_{\text{dust}}$  in the LMC by using some observational data (e.g., Bot et al. 2010; Skibba et al. 2012; Gordon et al. 2014). However, the total dust masses estimated are different: Using sub-millimeter excess of the LMC and fitting the dust models of Draine & Li (2007), Bot et al. (2010) obtained  $M_{\text{dust}}$  of  $3.6 \times 10^6 M_{\odot}$ ; According to *Herschel* HERITAGE data, Skibba et al. (2012) predicted  $M_{\text{dust}} \sim 1.1 \times 10^6 M_{\odot}$ ; Based on the HERITAGE *Herschel* Key Project photometric data, Gordon et al. (2014) obtained  $M_{\text{dust}}$  of  $7.3 \times 10^5 M_{\odot}$ , which is a factor of about 5 lower than previous results. These differences maybe come from different dust models, the fitting techniques, the wavelength range, and the factor of environments (Gordon et al. 2014). As Figure 10 shows, the total dust mass produced by AGB stars or CE ejecta is much lower than the above observational estimates. Of course, we do not know whether dust produced by SNe II is dominant because theoretical models and observational estimates can hardly give any certain value for the dust yields of SNe II.

Furthermore, dust grains can be destroyed by the blast wave produced by SNe. Therefore, their existence should have time scale. According to the properties of the dust material and the occurrence rate of SNe in the LMC, Zhukovska & Henning (2013) estimated the time scale of dust destruction. They found that the time scale for silicate grains is about 0.8 Gyr, and it is about 1.1 Gyr for carbonaceous grains. This means that about 10% of dust masses showed in Figure 10 can survive if we consider the dust destruction. It is possible that AGB stars and CE ejecta

are not main dust sources and dust can grow in the ISM of the LMC (Draine 2009).

As discussed in Introduction, according to the estimates of Weingartner & Draine (2001), we indirectly guess that the mass ratio of carbon to silicate grains in the LMC is about 1:4. However, to our knowledge, there is no direct observations to give the compositions of different dust species in the LMC. It is very important for us to understand the dust origin. We theoretically predict the time evolution of accumulated masses of different dust species from CE ejecta and AGB stars in Figure 11. Obviously, in the model of Zhukovska & Henning (2013), most of dust grains are carbon and others are negligible. In the model of new ATON, the mass fractions of carbon and silicate grains are about 82% and 13%, respectively, and the left are mainly SiC grains. In the model of old ATON, the mass fractions of carbon and silicate grains are about 55% and 35%, respectively. The remaining are SiC and iron grains. However, in CE ejecta, about 50% of dust grains are silicate, 20% of them are iron and the mass fractions of carbon and SiC grains are about 17% and 13%, respectively. Not like AGB stars which mainly form C-rich grains, CE ejecta chiefly produces O-rich dust grains.

Therefore, with the further observations, we believe that the compositions of different dust species in the LMC will be found soon. Then, we can estimate which between AGB stars and CE ejecta is more important dust source. Of course, we also should consider the effect of SNe II and dust growth in the ISM.

## 5 CONCLUSIONS

In this work, we calculate the contributions of dust produced by AGB stars, CE ejecta and SNe II to the total dust budget in the LMC. Because different observations still have large scatter and theoretical models greatly depend on complex physical processes, we can not determine which is the main dust source in the LMC. However, more than 50% of stars in the LMC are in binary systems. Many of them may have or will undergo CE evolutions. According to our model, CE ejecta can efficiently produce dust. Therefore, we must consider the contributions of dust produced by CE ejecta on estimating the total dust budget.

In our simulations, the DPRs of AGB stars in the LMC are between about  $2.5 \times 10^{-5} M_{\odot} \text{yr}^{-1}$  and  $4.0 \times 10^{-6} M_{\odot} \text{yr}^{-1}$ . The uncertainty mainly results from different models for the dust yields of AGB stars. These results are within the large scatter of several observational estimates. The DPRs of CE ejecta are about  $6.3 \times 10^{-6} M_{\odot} \text{yr}^{-1}$  (The initial binary fraction is 50%). Compared the theoretically predicted DPRs of AGB stars, the DPRs of CE ejecta are significant or dominated. The contribution of SNe II is very uncertain. Compared with SNe II without reverse shock, the DPRs of AGB stars and CE ejecta are negligible. However, if only 2 % of dust grains produced by SNe II can survive after reverse shock, the contribution of SNe II is very small.

The total dust mass of the LMC estimated by observations is between  $7.3 \times 10^5 M_{\odot}$  and  $3.6 \times 10^6 M_{\odot}$ . In our work, the total dust mass produced by AGB stars in different models are between  $2.8 \times 10^4 M_{\odot}$  and  $3.2 \times 10^5 M_{\odot}$ , and those produced by CE ejecta are about  $6.3 \times 10^4 M_{\odot}$ . In

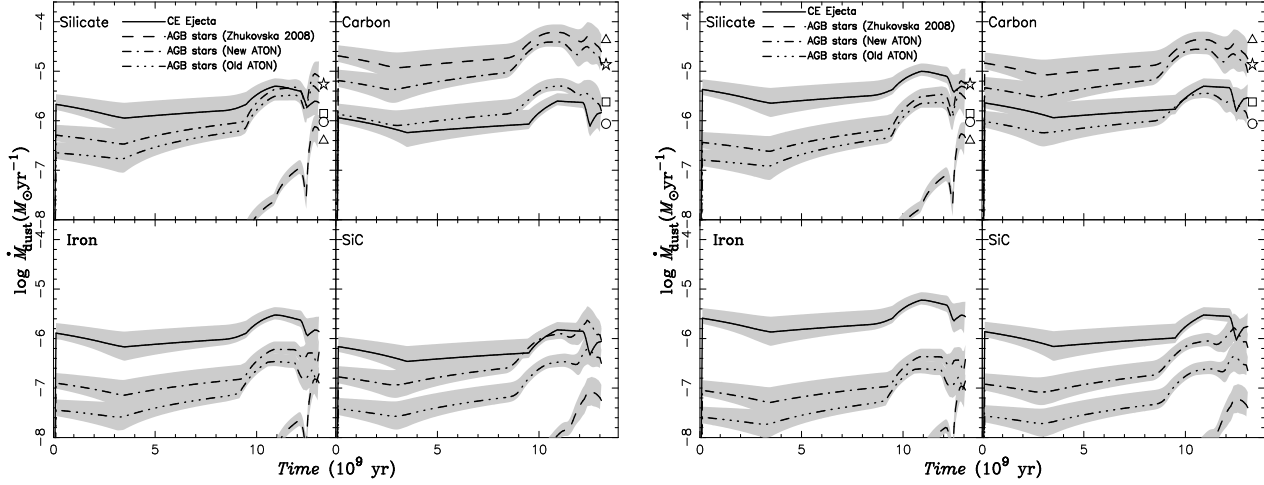


**Figure 8.** The dust production rates (DPRs) of different dust species from CE ejecta and AGB stars in the LMC as a function of time for metallicity-dependent star formation histories given by Harris & Zaritsky (2009). Left and right panels show that the initial binary fractions are 50% and 100%, respectively. The solid, dashed, dash-dotted and dot-dot-dot-dashed lines show the predicted DPRs from CE ejecta, AGB stars using the dust yields of Zhukovska et al. (2008), new and old ATON, respectively. The shaded regions around lines represent the uncertainty on the best-fit star formation histories. The DPRs of O-rich and C-rich AGB stars observationally estimated by Matsuura et al. (2009), Srinivasan et al. (2009), Boyer et al. (2012) and Riebel et al. (2012) are represented by triples, stars, squares, and circles, respectively.

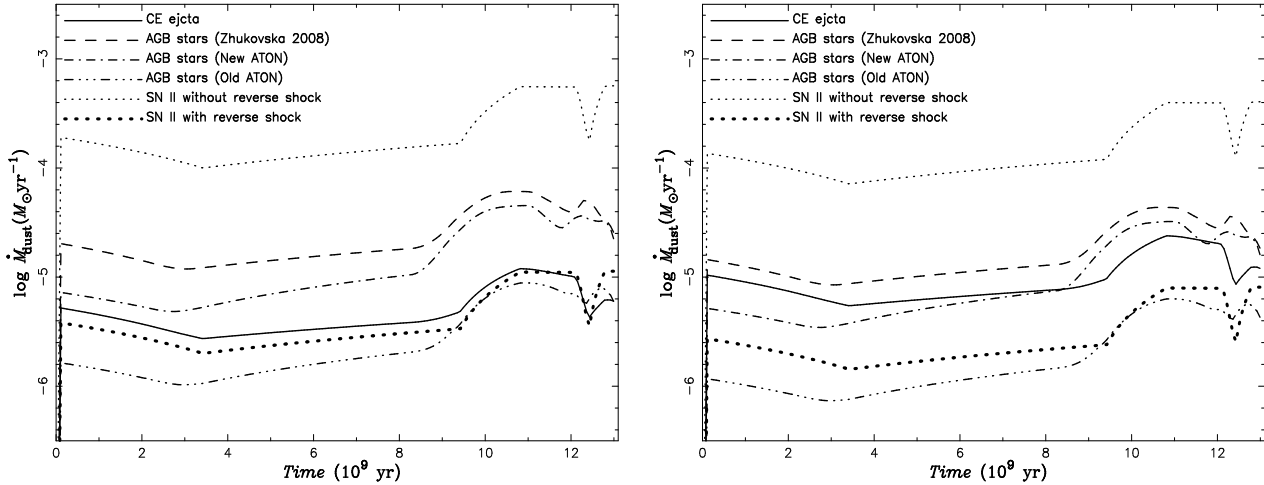


**Figure 9.** The total DPRs from CE ejecta, AGB stars and SNe II with the age of the LMC by using the best-fit star formation histories. Left and right panels show that the initial binary fractions are 50% and 100%, respectively. The solid, dashed, dash-dotted and dot-dot-dot-dashed lines show the predicted DPRs from CE ejecta, AGB stars using the dust yields of Zhukovska et al. (2008) and the new ATON in Schneider et al. (2014), respectively. Thin dotted lines represent the DPRs from SNe II using the dust yields of Todini & Ferrara (2001), while thick dotted lines use 2% of the dust yields of Todini & Ferrara (2001).

our calculations, the total dust masses produced by SNe II are very uncertain, and they change from  $2.8 \times 10^3 M_\odot$  to  $2.8 \times 10^6 M_\odot$ . If the destruction of blast wave from SNe is considered, compared with the observational estimates, the total dust masses produced by AGB stars, CE ejecta and SNe II are negligible. Therefore, on estimating the total dust mass, the growth of dust in the ISM must be considered.

Not only observational estimates but also theoretical predictions found that AGB stars in the LMC mainly produce carbon grains. Based on our simulations, most of dust grains forming in CE ejecta are silicate and iron grains. Therefore, with the further observations, the compositions

of different dust species will be found, which may be very important for understanding the dust origins and the contributions of dust produced by AGB stars and CE ejecta.

## ACKNOWLEDGMENTS

We thank an anonymous referee for his/her comments which helped to improve the paper. This work was supported by XinJiang Science Fund for Distinguished Young Scholars under Nos. 2014721015 and 2013721014, the National Natural Science Foundation of China under Nos. 11473024, 11363005 and 11163005.

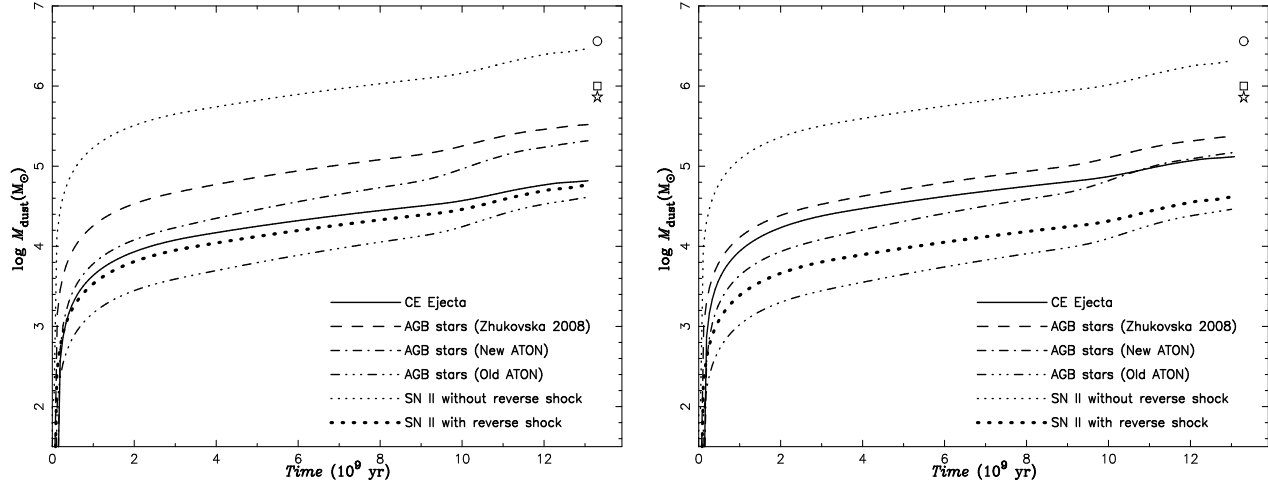


**Figure 10.** Similar with Figure 9, but for time evolution of total dust masses from CE ejecta, AGB stars and SNe II. The observational estimates presented by circle, square and star are taken from Bot et al. (2010), Skibba et al. (2012) and Gordon et al. (2014), respectively.

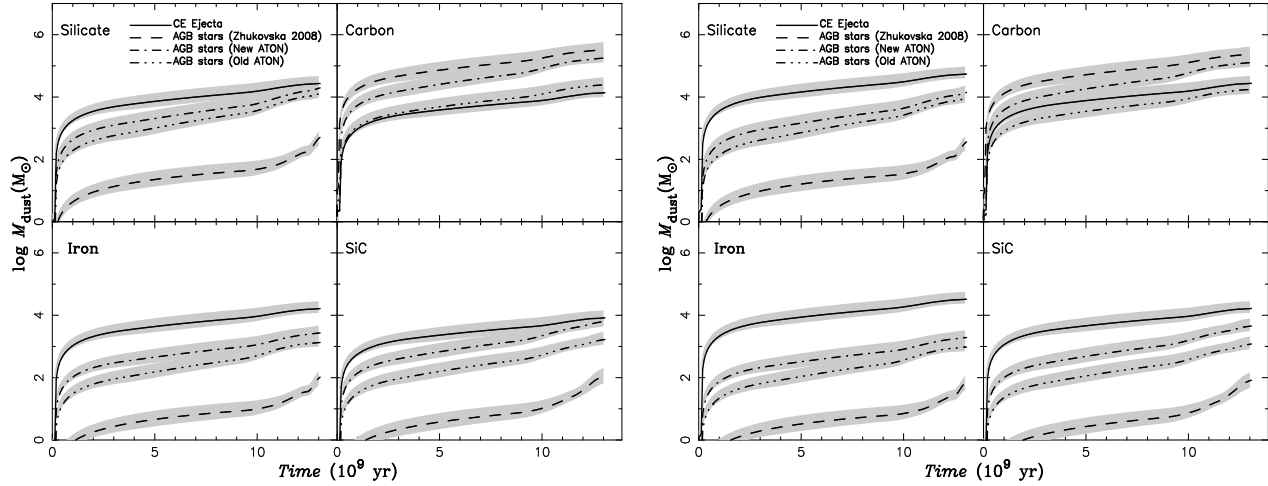


**Figure 11.** Similar with Figure 8, but for time evolution of accumulated masses of different dust species from CE ejecta and AGB stars.

## REFERENCES

- Anders E., Grevesse N., 1989, *Grochim. Cosmochim. Acta*, 53, 197
- Bianchi S., Schneider R., 2007, *MNRAS*, 378, 973
- Blum R. D., Mould J. R., Olsen K. A., Frogel J. A., Werner M., Meixner M., Markwick-Kemper F., Indebetouw R., Whitney B., 2006, *AJ*, 132, 2034
- Borkowski K. J., Williams B. J., Reynolds S. P., Blair W. P., Ghavamian P., Sankrit R., Hendrick S. P., Long K. S., Raymond J. C., Smith R. C., Points S., Winkler P. F., 2006, *ApJL*, 642, L141
- Bot C., Ysard N., Paradis D., Bernard J. P., Lagache G., Israel F. P., Wall W. F., 2010, *A&A*, 523, A20
- Boyer M. L., Srinivasan S., Riebel D., McDonald I., van Loon J. T., Clayton G. C., Gordon K. D., Meixner M., Sargent B. A., Sloan G. C., 2012, *ApJ*, 748, 40
- Cioni M.-R. L., van der Marel R. P., Loup C., Habing H. J., 2000, *A&A*, 359, 601
- Dell’Agli F., Ventura P., García Hernández D. A., Schneider R., Di Criscienzo M., Brocato E., D’Antona F., Rossi C., 2014, *MNRAS*, 442, L38
- Dell’Agli F., Ventura P., Schneider R., Di Criscienzo M., García-Hernández D. A., Rossi C., Brocato E., 2015, *ArXiv e-prints*
- Di Criscienzo M., Dell’Agli F., Ventura P., Schneider R., Valiante R., La Franca F., Rossi C., Gallerani S., Maiolino R., 2013, *MNRAS*, 433, 313
- Draine B. T., 2009, in Henning T., Grün E., Steinacker J., eds, *Cosmic Dust - Near and Far Vol. 414 of Astronomical Society of the Pacific Conference Series, Interstellar Dust Models and Evolutionary Implications*. p. 453
- Draine B. T., Li A., 2007, *ApJ*, 657, 810
- Draine B. T., Salpeter E. E., 1979, *ApJ*, 231, 438
- Dunne L., Eales S., Ivison R., Morgan H., Edmunds M., 2003, *Nature*, 424, 285
- Dwek E., 1998, *ApJ*, 501, 643
- Dwek E., Galliano F., Jones A. P., 2007, *ApJ*, 662, 927
- Egan M. P., Van Dyk S. D., Price S. D., 2001, *AJ*, 122, 1844
- Eggleton P. P., 1971, *MNRAS*, 151, 351

- Eggleton P. P., 1972, *MNRAS*, 156, 361
- Eggleton P. P., Faulkner J., Flannery B. P., 1973, *A&A*, 23, 325
- Eldridge J. J., Izzard R. G., Tout C. A., 2008, *MNRAS*, 384, 1109
- Feder J., Russell K. C., Lothe J., Pound G. M., 1966, *Advances in Physics*, 15, 111
- Ferrarotti A. S., Gail H., 2003, *A&A*, 398, 1029
- Ferrarotti A. S., Gail H., 2006, *A&A*, 447, 553
- Fransson C., Chevalier R. A., 1989, *ApJ*, 343, 323
- Gail H., Sedlmayr E., 1999, *A&A*, 347, 594
- Gail H.-P., Zhukovska S. V., Hoppe P., Trieloff M., 2009, *ApJ*, 698, 1136
- Gall C., Hjorth J., Andersen A. C., 2011, *A&A Rev.*, 19, 43
- Goldberg D., Mazeh T., 1994, *A&A*, 282, 801
- Gordon K. D., Roman-Duval J., Bot C., et al. 2014, *ApJ*, 797, 85
- Groenewegen M. A. T., de Jong T., 1993, *A&A*, 267, 410
- Han Z., Podsiadlowski P., Eggleton P. P., 1994, *MNRAS*, 270, 121
- Harris J., Zaritsky D., 2009, *AJ*, 138, 1243
- Hashimoto A., 1990, *Nature*, 347, 53
- Herwig F., 2005, *ARA&A*, 43, 435
- Hurley J. R., Tout C. A., Pols O. R., 2002, *MNRAS*, 329, 897
- Iben Jr. I., Livio M., 1993, *PASP*, 105, 1373
- Iben Jr. I., Renzini A., 1983, *ARA&A*, 21, 271
- Ita Y., Onaka T., Kato D., et al. 2008, *PASJ*, 60, 435
- Izzard R. G., Tout C. A., Karakas A. I., Pols O. R., 2004, *MNRAS*, 350, 407
- Karakas A. I., Lattanzio J. C., Pols O. R., 2002, *PASA*, 19, 515
- Kashi A., Soker N., 2011, *MNRAS*, 417, 1466
- Kozasa T., Hasegawa H., Nomoto K., 1989, *ApJ*, 344, 325
- Kraicheva Z. T., Popova E. I., Tutukov A. V., Yungelson L. R., 1989, *Astrophysics*, 30, 323
- Lü G., Zhu C., Han Z., Wang Z., 2008, *ApJ*, 683, 990
- Lü G., Zhu C., Podsiadlowski P., 2013, *ApJ*, 768, 193
- Marigo P., Girardi L., 2007, *A&A*, 469, 239
- Massey P., Plez B., Levesque E. M., Olsen K. A. G., Clayton G. C., Josselin E., 2005, *ApJ*, 634, 1286
- Matsuura M., Barlow M. J., Zijlstra A. A., Whitelock P. A., Cioni M.-R. L., Groenewegen M. A. T., Volk K., Kemper F., Kodama T., Lagadec E., Meixner M., Sloan G. C., Srinivasan S., 2009, *MNRAS*, 396, 918
- McDonald I., Boyer M. L., van Loon J. T., Zijlstra A. A., Hora J. L., Babler B., Block M., Gordon K., Meade M., Meixner M., Misselt K., Robitaille T., Sewilo M., Shiao B., Whitney B., 2011, *ApJS*, 193, 23
- McDonald I., van Loon J. T., Decin L., Boyer M. L., Dupree A. K., Evans A., Gehrz R. D., Woodward C. E., 2009, *MNRAS*, 394, 831
- Meixner M., Gordon K. D., Indebetouw R., et al. 2006, *AJ*, 132, 2268
- Nagahara H., Ozawa K., 1996, *Grochim. Cosmochim. Acta*, 60, 1445
- Nicholls C. P., Melis C., Soszyński I., Udalski A., Szymański M. K., Kubiak M., Pietrzyński G., Poleski R., Ulaczyk K., Wyrzykowski L., Kozłowski S., Pietrukowicz P., 2013, *MNRAS*, 431, L33
- Nozawa T., Kozasa T., Umeda H., Maeda K., Nomoto K., 2003, *ApJ*, 598, 785
- Nozawa T., Maeda K., Kozasa T., Tanaka M., Nomoto K., Umeda H., 2011, *ApJ*, 736, 45
- Paczynski B., 1976, in Eggleton P., Mitton S., Whelan J., eds, *Structure and Evolution of Close Binary Systems Vol. 73 of IAU Symposium, Common Envelope Binaries*. p. 75
- Riebel D., Srinivasan S., Sargent B., Meixner M., 2012, *ApJ*, 753, 71
- Schneider R., Valiante R., Ventura P., dell Agli F., Di Criscienzo M., Hirashita H., Kemper F., 2014, *ArXiv e-prints*
- Sharp C. M., Huebner W. F., 1990, *ApJS*, 72, 417
- Shimonishi T., Onaka T., Kato D., Sakon I., Ita Y., Kawamura A., Kaneda H., 2013, *AJ*, 145, 32
- Skibba R. A., Engelbracht C. W., Aniano G., et al. 2012, *ApJ*, 761, 42
- Srinivasan S., Meixner M., Leitherer C., et al. 2009, *AJ*, 137, 4810
- Todini P., Ferrara A., 2001, *MNRAS*, 325, 726
- Tout C. A., Zytow A. N., Church R. P., Lau H. H. B., 2014, *ArXiv e-prints*
- Ventura P., Criscienzo M. D., Schneider R., Carini R., Valiante R., D'Antona F., Gallerani S., Maiolino R., Tornambé A., 2012, *MNRAS*, 424, 2345
- Ventura P., Dell'Agli F., Schneider R., Di Criscienzo M., Rossi C., La Franca F., Gallerani S., Valiante R., 2014, *MNRAS*, 439, 977
- Ventura P., di Criscienzo M., Schneider R., Carini R., Valiante R., D'Antona F., Gallerani S., Maiolino R., Tornambé A., 2012, *MNRAS*, 420, 1442
- Weingartner J. C., Draine B. T., 2001, *ApJ*, 548, 296
- Zhu C., Lü G., Wang Z., 2013, *ApJ*, 777, 23
- Zhukovska S., Gail H.-P., Trieloff M., 2008, *A&A*, 479, 453
- Zhukovska S., Henning T., 2013, *A&A*, 555, A99

This paper has been typeset from a  $\text{\LaTeX}$  file prepared by the author.